Human Molecular Genetics, 2013, Vol. 22, No. 5 **852–866**
doi:10.1093/hmg/dds490
Advance Access published on November 21, 2012

Hippocampal dysfunction in the *Euchromatin histone methyltransferase 1* heterozygous knockout mouse model for Kleefstra syndrome

Monique C.M. Balemans[1,2], Nael Nadif Kasri[3], Maksym V. Kopanitsa[5], Nurudeen O. Afinowi[5], Ger Ramakers[6], Theo A. Peters[4], Andy J. Beynon[4], Sanne M. Janssen[1], Rik C.J. van Summeren[1,2], Jorine M. Eeftens[1], Nathalie Eikelenboom[1], Marco Benevento[3], Makoto Tachibana[7], Yoichi Shinkai[7], Tjitske Kleefstra[1], Hans van Bokhoven[1,3,*,†] and Catharina E.E.M. Van der Zee[2,*,†]

[1]Department of Human Genetics, [2]Department of Cell Biology, Nijmegen Centre for Molecular Life Sciences, [3]Department of Cognitive Neurosciences, and [4]Department of Otorhinolaryngology, Donders Institute for Brain, Cognition and Behavior, Radboud University, Nijmegen Medical Centre, P.O. Box 9101, 6500 HB Nijmegen, the Netherlands [5]Synome Ltd, Moneta Building, Babraham Research Campus, Cambridge CB22 3AT, UK, [6]Department of Developmental Psychology, University of Amsterdam, Roetersstraat 15, 1018 WB Amsterdam, the Netherlands and [7]Experimental Research Center for Infectious Diseases, Institute for Virus Research, Kyoto, University, 53 Shogoin, Kawara-cho, Sakyo-ku, Kyoto, Japan

Received October 21, 2012; Revised October 21, 2012; Accepted November 15, 2012

Euchromatin histone methyltransferase 1 (EHMT1) is a highly conserved protein that catalyzes mono- and dimethylation of histone H3 lysine 9, thereby epigenetically regulating transcription. Kleefstra syndrome (KS), is caused by haploinsufficiency of the *EHMT1* gene, and is an example of an emerging group of intellectual disability (ID) disorders caused by genes encoding epigenetic regulators of neuronal gene activity. Little is known about the mechanisms underlying this disorder, prompting us to study the *Euchromatin histone methyltransferase 1* heterozygous knockout (*Ehmt1*$^{+/-}$) mice as a model for KS. In agreement with the cognitive disturbances observed in patients with KS, we detected deficits in fear extinction learning and both novel and spatial object recognition in *Ehmt1*$^{+/-}$ mice. These learning and memory deficits were associated with a significant reduction in dendritic arborization and the number of mature spines in hippocampal CA1 pyramidal neurons of *Ehmt1*$^{+/-}$ mice. In-depth analysis of the electrophysiological properties of CA3-CA1 synapses revealed no differences in basal synaptic transmission or theta-burst induced long-term potentiation (LTP). However, paired-pulse facilitation (PPF) was significantly increased in *Ehmt1*$^{+/-}$ neurons, pointing to a potential deficiency in presynaptic neurotransmitter release. Accordingly, a reduction in the frequency of miniature excitatory post-synaptic currents (mEPSCs) was observed in *Ehmt1*$^{+/-}$ neurons. These data demonstrate that *Ehmt1* haploinsufficiency in mice leads to learning deficits and synaptic dysfunction, providing a possible mechanism for the ID phenotype in patients with KS.

INTRODUCTION

Euchromatin histone methyltransferase 1 (*EHMT1*) is a highly conserved gene. In mice, *Ehmt1* shows 97% homology in the amino acid sequence compared with its human orthologue. Ehmt1, also called G9a-like protein (GLP) or KMT1D, forms a heteromeric complex with Ehmt2/G9a/KMT1C to catalyze mono- and dimethylation of lysine 9 of the histone

*To whom correspondence should be addressed. Tel: +31 243614296; Fax: +31 243615317; Email: i.vanderzee@ncmls.ru.nl (C.E.E.M. Van der Zee); Tel: +31 243616696; Fax: +31 243668752; Email: h.vanbokhoven@gen.umcn.nl (H. van Bokhoven)
†These authors contributed equally to the manuscript.

H3 N-terminal tail (H3K9me2) in euchromatic DNA (1), an epigenetic mark for transcriptional silencing (2,3). Furthermore, Ehmt1 and Ehmt2 function in larger protein complexes with Wiz, CtBP1 and CtBP2 (4) and other H3K9 methyltransferases Suv39h1/KMT1A and SETDB1/KMT1E (5) to repress transcription.

Loss-of-function mutations or deletions of *EHMT1*, leading to haploinsufficiency of this gene, cause a recognizable human intellectual disability (ID) syndrome called Kleefstra Syndrome (KS; OMIM #610253) (6–8). Core features are ID, general developmental delay, childhood hypotonia and craniofacial abnormalities (9). Furthermore, autistic-like behavioural problems and cardiac defects are common in these patients. Although KS was defined only a few years ago (7), there are already 112 reported patients, and it is thought to be one of the most common subtelomeric deletion syndromes (9,10). Interestingly, in a recent study we identified mutations in the *MLL3*, *SMARCB1*, *NR1I3* and *MBD5* genes in patients with a KS phenotype who lacked mutations in the *EHMT1* gene (11). These genes encode epigenetic regulators and were shown to interact with EHMT1, implying an epigenetic network important for cognitive abilities. Indeed, KS is an example of an emerging group of ID disorders that are caused by genes encoding epigenetic regulators of neuronal gene activity (12–14). In addition, EHMT1 mutations have recently been identified across diagnostic boundaries, i.e. in ID, autism spectrum disorder and schizophrenia (15–17).

In mice, homozygous *Ehmt1* deficiency leads to embryonic lethality, whereas heterozygous *Ehmt1*$^{+/-}$ mice are viable and fertile (1,18). Recently, we have reported that *Ehmt1*$^{+/-}$ mice show hypoactivity, reduced exploration, increased anxiety and aberrant social behaviour when compared with their wild-type littermates (18). This recapitulates the autistic-like features and hypoactivity seen in KS patients (19–21), making the *Ehmt1*$^{+/-}$ mouse a good mammalian model for this syndrome, with construct and face validity.

Despite the critical role that EHMT1 plays in human cognitive function, relatively little is known about its contribution to nervous system development or how loss of EHMT1 function leads to cognitive impairments seen in KS. Recent studies have started to shed light on the role of EHMT1 in learning and memory. Memory deficits were revealed using a fear conditioning paradigm in mice with a homozygous *Ehmt1* knockout in postnatal forebrain neurons (22). Consistent with our previous observations, these mice also showed hypoactivity and reduced exploration of a novel environment (18,22). Further convincing evidence for the role of EHMT1 in learning and memory comes from a recent study in *Drosophila* that identified EHMT as a key regulator of classic learning and memory genes (23). Mutant flies that did not express EHMT showed deficits in several memory paradigms and significantly reduced dendritic branching of multidendrite neurons of the larval body wall (23).

In this study, we sought to understand whether and how *Ehmt1* haploinsufficiency in mice leads to cognitive dysfunction. We found that *Ehmt1*$^{+/-}$ mice displayed deficits in fear conditioned extinction learning and both the novel and spatial object recognition tests. At the morphological level, we observed reduced branching and spine density in *Ehmt1*$^{+/-}$ CA1 hippocampal neurons. Finally, electrophysiological recordings of CA3-CA1 synapses showed presynaptic defects. These data demonstrate a crucial role for Ehmt1 in synaptic transmission, and suggest that KS may arise from a defect in synaptic function.

RESULTS

Ehmt1 protein expression decreases rapidly after birth

To start understanding the function of Ehmt1 in learning and memory, we first performed a detailed analysis of Ehmt1 protein expression patterns from early postnatal development throughout the entire lifespan of wild-type and *Ehmt1*$^{+/-}$ mice, a construct valid model for KS (1). Interestingly, Ehmt1 levels were initially high at P4 and showed an ~10-fold reduction within the first month after birth in wild-type mouse brain ($P < 0.001$; Fig. 1A). In addition, the levels in *Ehmt1*$^{+/-}$ brains were significantly reduced by ~40–50% compared with wild-type at the age of 4 days ($P < 0.007$), 8 days ($P < 0.001$), 14 days ($P < 0.001$) and 1 month ($P < 0.012$; Fig. 1A), confirming that haploinsufficiency of the *Ehmt1* gene leads to a strong reduction in protein levels. From 1 month of age onwards, Ehmt1 levels were at a constant low level in both cortex (Fig. 1B) and hippocampus (Fig. 1C) up to 20 months of age. Notably, the significantly diminished expression in *Ehmt1*$^{+/-}$ mice was observed at all ages in cortex (1 m: $P < 0.049$; 3 m: $P < 0.013$; 10 m: $P < 0.007$; 20 m: $P < 0.002$; Fig. 1B) and hippocampus (1 m: $P < 0.013$; 3 m: $P < 0.022$; 10 m: $P < 0.002$; 20 m: $P < 0.029$; Fig. 1C). The strong decrease in protein levels within the first month after birth implies that Ehmt1 plays a role in the developing brain. However, when we examined the gross morphology of the hippocampus in adult mice of 1, 3, 10 and 20 months of age, no apparent differences in layering were observed between wild-type and *Ehmt1*$^{+/-}$ mice (Fig. 1D).

Ehmt1$^{+/-}$ mice are not affected in Barnes maze spatial learning and memory

Because of the severe ID in KS patients and the expression of Ehmt1 in mouse hippocampus, we assessed learning and memory abilities of *Ehmt1*$^{+/-}$ mice in multiple learning and memory tests. Spatial navigation was tested in the Barnes maze (33,34). The mice were subjected to repetitive training by means of 17 learning trials, with the escape hole at a fixed position with respect to the spatial cues, and the other holes being closed (Fig. 2A). During acquisition both genotypes showed a learning curve, with decreasing escape latencies (Fig. 2B). The subsequent probe test, with all 12 holes closed, revealed a high preference for the escape quadrant (SE) by wild-type and *Ehmt1*$^{+/-}$ mice, indicating no genotype differences in memory of the previous escape location (Fig. 2C). A long-term memory probe test was performed 7 days later, again showing escape quadrant preferences in both genotype groups (Fig. 2D).

We then performed the Barnes maze paradigm with another group of animals that were older (9–11 months) than the first

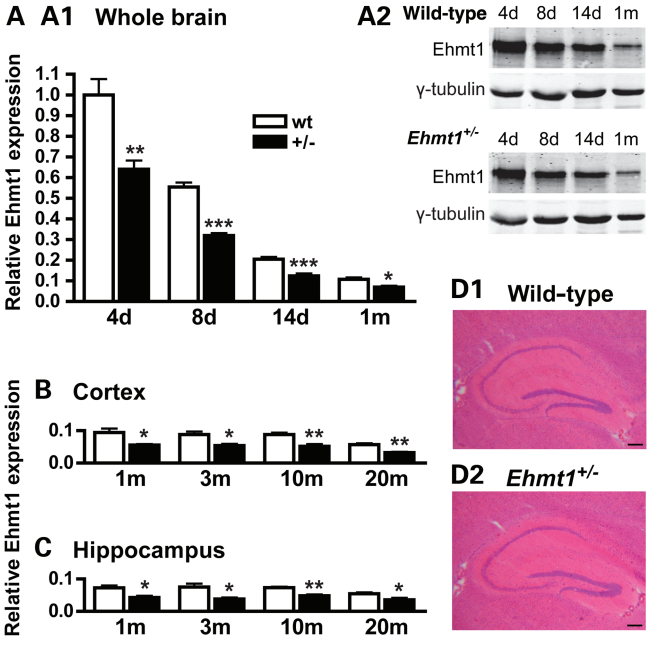

Figure 1. Ehmt1 expression levels decrease significantly with age. (**A1**) Ehmt1 protein levels of 4, 8, 14 days and 1 month old wild-type ($n = 4–5$) and *Ehmt1*$^{+/-}$ ($n = 4–5$) mice were initially high (postnatal day 4 set at 1.0) and decreased with age. In addition, protein levels of *Ehmt1*$^{+/-}$ mice were significantly reduced. (**A2**) shows representative western blots. (**B**) Ehmt1 protein levels in the cortex of adult mice remain at a constant lower level at 1, 3, 10 and 20 months, compared with the younger ages. (**C**) Ehmt1 protein levels in hippocampus of adult mice also remain at a low level from 1 until 20 months of age. (**D**) Representative images of hematoxylin and eosin stained hippocampus sections of 3 months old wild-type (**D1**) and *Ehmt1*$^{+/-}$ mice (**D2**), showing no gross morphological abnormalities. $^{*}P < 0.05$, $^{**}P < 0.01$, $^{***}P < 0.001$, bar = 200 μm.

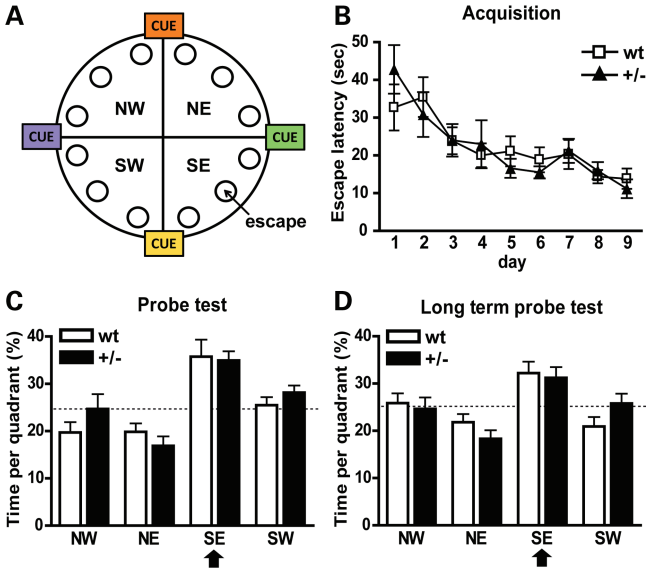

Figure 2. Spatial learning and memory characteristics of *Ehmt1*$^{+/-}$ mice in the Barnes maze. (**A**) Wild-type ($n = 12$) and *Ehmt1*$^{+/-}$ ($n = 12$) mice had to learn the location of the escape hole, located in the middle hole of the SE quadrant, by using distant visual spatial cues. (**B**) Both genotypes showed comparable and decreasing escape latencies during acquisition. (**C**) During the subsequent probe test, with all 12 holes closed, both groups showed a high preference for the escape quadrant. (**D**) A long-term probe test, 7 days later, revealed no genotype differences. The arrows indicate the SE escape quadrant for the probe tests.

group (4 months). The acquisition learning curves of the older wild-type and *Ehmt1*$^{+/-}$ groups were highly similar to those of the younger group (data not shown). The escape quadrant preferences during the probe test (wild-type 41.2 ± 2.2%, *Ehmt1*$^{+/-}$ 43.9 ± 2.5%) and long-term probe test (wild-type 35.1 ± 2.7%, *Ehmt1*$^{+/-}$ 36.7 ± 4.1%) were also similar to the younger group, with no genotype differences revealed. This older group subsequently performed a reversal learning paradigm, during which the escape hole was relocated to the middle hole of the SW quadrant. Still, no learning and memory impairments in the *Ehmt1*$^{+/-}$ mice were revealed (wild-type 38.9 ± 3.5%, *Ehmt1*$^{+/-}$ 41.8 ± 4.7% SW escape quadrant preference). Together, these data show that after repetitive training trials in the Barnes maze, *Ehmt1*$^{+/-}$ mice have spatial learning and memory capabilities that are similar to their wild-type littermates.

Ehmt1$^{+/-}$ mice show impaired fear conditioned extinction, and an increased sensitivity to external stimuli

We evaluated associative learning in *Ehmt1*$^{+/-}$ mice by using a fear conditioning paradigm. This form of learning is studied and observed in many species, including rodents and humans, involving multiple brain areas, including the hippocampus, amygdala and prefrontal cortex (35–39). Here, we studied both contextual and cued fear conditioning, and cued fear extinction. During the acquisition phase, the animals received a total of four footshocks that were each preceded by a 30 s tone. The time the mice spent freezing was measured as an indicator for learning and memory. Wild-type and *Ehmt1*$^{+/-}$ mice displayed no freezing during the exploration phase and the first 30 s tone, when no footshock had been applied (Fig. 3A). After the first footshock, freezing increased gradually during acquisition (Fig. 3A). Interestingly, *Ehmt1*$^{+/-}$ mice displayed twice as much freezing compared with wild-type during this acquisition phase ($F_{1,21} = 15.256$, $P < 0.001$; Fig. 3A). During the context test, 24 h after acquisition, wild-type and *Ehmt1*$^{+/-}$ mice displayed freezing behaviour, indicating that they learned the association between the context and the aversive stimulus. *Ehmt1*$^{+/-}$ mice again showed twice as much freezing compared with wild-types ($P < 0.017$; Fig. 3B), but for each group the context test freezing level was comparable with the acquisition freezing level. During the tone test, which was performed 48 h after acquisition in a different context, tone presentation induced freezing behaviour. Pre-tone freezing was higher in *Ehmt1*$^{+/-}$ mice ($P < 0.008$). During tone presentations however, we did not observe any significant differences between genotypes (Fig. 3B). We then assessed the ability of mice to extinguish a conditioned response to the cue by means of extinction training. This active form of learning (40) depends upon interactions between the prefrontal cortex and amygdala (41), whereas the hippocampus influences contextual modulation of extinction (42). Training was performed by administering five tones per session per day, during 6 days (Fig. 3C). On extinction day 1, wild-type mice demonstrated decreased

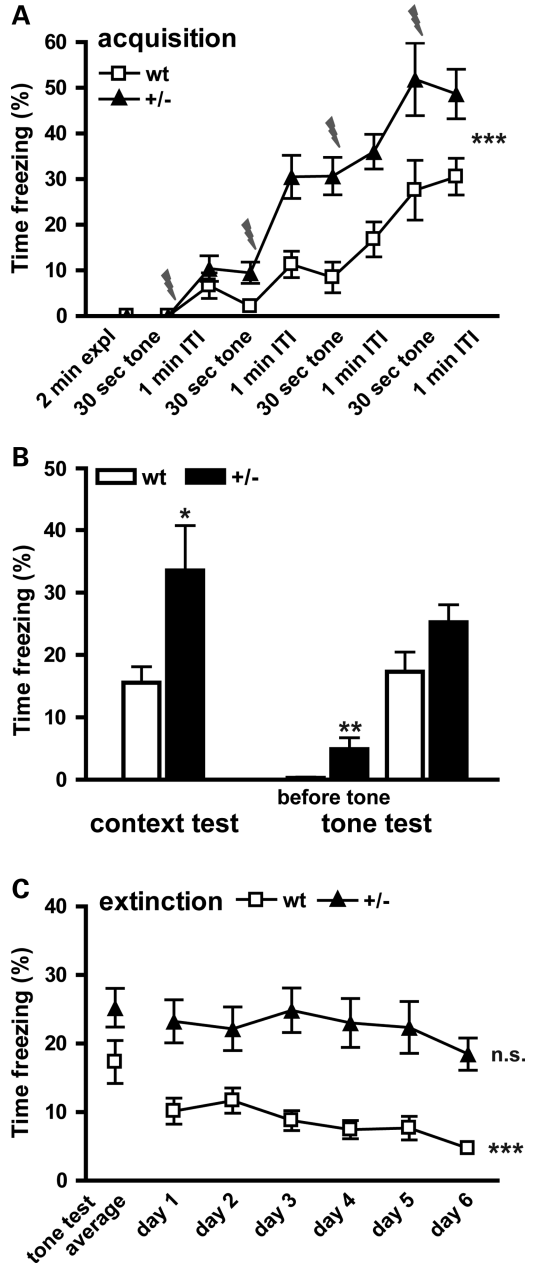

Figure 3. Increased sensitivity and impaired fear extinction learning in *Ehmt1*$^{+/-}$ mice. The % time freezing levels of wild-type ($n = 13$) and *Ehmt1*$^{+/-}$ ($n = 10$) mice during the fear conditioning test. (**A**) During acquisition mice received a total of four footshocks, indicated by grey flashes, at the end of each 30 s tone period. Freezing increased gradually during the trial, with significantly increased freezing in the *Ehmt1*$^{+/-}$ mice. (**B**) Context memory was tested for 5 min, 24 h after acquisition, during which the freezing levels were significantly higher in *Ehmt1*$^{+/-}$ mice. Tone memory was tested 48 h after acquisition, in an alternate context. After the first tone, freezing levels increased indicating that both genotypes learned the association, but without revealing significant differences between the two groups. (**C**) Tone extinction started 5 days after acquisition, in the alternate context. Each session contained five 30 s tones, each followed by a 1 min ITI. Values are averaged per session. Wild-type mice showed a significant decrease in freezing levels from day 1–6; however, this was not observed for the *Ehmt1*$^{+/-}$ mice. $^{*}P < 0.05$, $^{**}P < 0.01$, $^{***}P < 0.001$, expl = exploration phase, ITI = intertrial interval.

freezing levels compared with the tone test. Furthermore, their freezing levels decreased significantly over time ($F_5 = 5.007$, $P < 0.001$) and were reduced by 53% on day 6 compared with day 1 (Fig. 3C). In contrast, *Ehmt1*$^{+/-}$ mice continued to demonstrate high freezing levels, which did not significantly decrease over time ($F_5 = 1.629$, $P < 0.172$), with only a 21% reduction from day 1 to day 6 (Fig. 3C). In summary, *Ehmt1*$^{+/-}$ mice showed increased freezing levels during acquisition and context testing, which might point to either enhanced associative learning or an increased sensitivity to sensory stimuli. For both the groups however, the context test freezing levels were comparable with their respective acquisition freezing levels, thus increased sensitivity is a more likely explanation. Interestingly, *Ehmt1*$^{+/-}$ mice showed decreased fear extinction compared with wild-types.

The heightened freezing response to footshock of the *Ehmt1*$^{+/-}$ mice may indicate an increased sensitivity to sensory stimuli. To investigate this further, mice were exposed to acoustic stimuli of increasing decibels (dB) and their startle response amplitude was measured (Table 1). Strikingly, *Ehmt1*$^{+/-}$ mice showed 60% increased startle responses for the 110, 120 and 130 dB pulses compared with wild-type (110 dB, $P < 0.021$; 120 dB, $P < 0.007$; 130 dB, $P < 0.011$; Table 1). To exclude any hearing difference between the genotypes, we investigated the auditory brainstem response (ABR) which revealed equal hearing abilities between wild-type and *Ehmt1*$^{+/-}$ mice (Table 1). The observations of (1) the enhanced freezing to footshock and (2) the amplified startle response to loud sound, together point to an increased sensitivity to external stimuli in the *Ehmt1*$^{+/-}$ mice.

Ehmt1$^{+/-}$ mice show impairments in the novel and spatial object recognition tasks

Given the increased sensitivity of *Ehmt1*$^{+/-}$ mice towards sensory stimuli, we next examined learning and memory behaviour without involvement of an aversive stimulus. To this end, we tested the *Ehmt1*$^{+/-}$ mice in two object recognition paradigms that rely on the animal's spontaneous exploratory behaviour (43–45). The novel and spatial object recognition tests require hippocampus function to a lesser and a greater extent, respectively (46–48). In the novel object recognition test (Fig. 4A), mice were tested for their ability to differentiate between a new object and a familiar one after different intertrial intervals (ITIs). In trial 2, wild-type mice spent significantly more time exploring the new object Q, compared with familiar object P, after 10 and 40 min ITIs (both $P < 0.001$; Table 2). However, after 80 min the wild-type mice did not show any preference for object Q anymore as demonstrated by equal 50% exploration times (Table 2). The absence of object preference after 80 min has also been observed in other studies with a 5 min pre-exposure (44,49). In contrast, *Ehmt1*$^{+/-}$ mice did not show any significant preference for object Q compared with object P after 10 and 80 min ITIs (Table 2). After 40 min ITI, the *Ehmt1*$^{+/-}$ mice spent significantly more time exploring the new object Q ($P < 0.016$; Table 2), which was similar to wild-type mice. To take into account the total exploration

Table 1. *Ehmt1*$^{+/-}$ mice have an increased sensitivity to acoustic stimuli in the startle response test

	Startle response (amplitude in arbitrary units) 70 dB	80 dB	90 dB	100 dB	110 dB	120 dB	130 dB
Wild-type	17.1 ± 0.7	15.6 ± 0.8	32.0 ± 5.8	90.1 ± 11.4	214.3 ± 24.7	340.2 ± 40.4	369.9 ± 37.7
Ehmt1$^{+/-}$	15.1 ± 0.8	16.1 ± 1.0	23.2 ± 3.8	116.3 ± 17.9	347.2 ± 45.8*	559.6 ± 58.1**	609.2 ± 74.1*

	ABR measurements (threshold in dB) Click	8 kHz	16 kHz	32 kHz
Wild-type	8.0 ± 3.2	32.0 ± 1.6	28.0 ± 4.3	50.0 ± 5.1
Ehmt1$^{+/-}$	13.7 ± 1.7	28.9 ± 3.1	23.3 ± 2.1	48.3 ± 3.1

Sensitivity to external stimuli was investigated by the acoustic startle reflex. *Ehmt1*$^{+/-}$ mice ($n = 9$) showed a significantly increased response to sound pulses of 110, 120 and 130 dB, compared with wild-types ($n = 9$). Background noise was at the level of 70 dB. ABR measurements showed no differences in hearing ability between the genotypes (wild-type $n = 5$, *Ehmt1*$^{+/-}$ $n = 8$). $^{*}P < 0.05$, $^{**}P < 0.01$, compared with wild-type, ABR = auditory brainstem response.

Table 2. *Ehmt1*$^{+/-}$ mice show impairments in the novel and spatial variants of the object recognition test

	Trial 2	Wild-type	*Ehmt1*$^{+/-}$
Novel object recognition 10 min ITI	Object P	25.6 ± 3.1%	42.3 ± 7.2%
	Object Q	74.4 ± 3.1%***	57.7 ± 7.2%
Novel object recognition 40 min ITI	Object P	36.3 ± 4.4%	39.2 ± 5.5%
	Object Q	63.7 ± 4.4%***	60.8 ± 5.5%*
Novel object recognition 80 min ITI	Object P	49.9 ± 4.1%	51.5 ± 7.7%
	Object Q	50.1 ± 4.1%	48.5 ± 7.7%
Spatial object recognition 60 min ITI	Object P1	38.0 ± 1.4%	47.8 ± 3.6%
	Object *chP2*	62.0 ± 1.4%***	52.2 ± 3.6%

Learning and memory abilities were tested with the novel ($n = 15$ wild-type and $n = 7$ *Ehmt1*$^{+/-}$ mice) and spatial ($n = 10$ wild-type and $n = 10$ *Ehmt1*$^{+/-}$ mice) object recognition tests. The specific exploration of each object during the 5 min trial 2 is shown in percentage of total exploration time. $^{*}P < 0.05$, $^{***}P < 0.001$, significantly more exploration of the new object Q compared with familiar object P, or the changed location object *chP2* compared with the non-displaced object P1 within one genotype group, ITI = intertrial interval.

activity, the *d*2 discrimination parameter was calculated (26). With this *d*2 value we were able to compare the genotype groups. *Ehmt1*$^{+/-}$ mice showed a significantly lower *d*2 value at 10 min ITI, confirming their reduced preference for the new object ($P < 0.021$; Fig. 4A).

In the spatial variant, the mice needed to discriminate between the new and the previous location of an object. Trial 2 was performed after a 60 min ITI, with object P2 being displaced (Fig. 4B). Wild-type mice demonstrated a significantly longer exploration of object P2 in the changed position (*chP2*), compared with object P1 ($P < 0.001$; Table 2). In contrast, *Ehmt1*$^{+/-}$ mice did not spend more time exploring *chP2*, compared with the non-displaced object P1, as shown by equal exploration times for both objects (Table 2). When comparing the genotype groups, *Ehmt1*$^{+/-}$ mice showed no discrimination of the displaced object *chP2*, in contrast to wild-type mice ($P < 0.021$; Fig. 4B). Of note, in both tasks we observed less exploration of *Ehmt1*$^{+/-}$ mice compared with wild-type mice, corroborating our previous observations (18).

Together, the data indicate that *Ehmt1*$^{+/-}$ mice show memory impairment in both novel and spatial object recognition. Combined with the observed deficits in conditioned fear extinction learning, our observations clearly demonstrate that *Ehmt1*$^{+/-}$ mice display significant learning and memory deficits.

Ehmt1$^{+/-}$ hippocampal neurons have reduced dendritic arborization and decreased spine density

Having established a role for Ehmt1 in learning and memory behaviour, we examined whether the learning and memory deficits in the *Ehmt1*$^{+/-}$ mice were associated with changes in neuronal morphology, as is the case for different ID syndromes (50–54). We performed an in-depth morphological analysis of Golgi-stained hippocampal CA1 pyramidal neurons. Branching phenotype of apical and basal dendrites was assessed by centrifugal ordering (Fig. 5A). When compared with wild-type, *Ehmt1*$^{+/-}$ neurons showed a reduced total length ($P < 0.050$; Fig. 5B), reduced number of branch parts ($P < 0.049$; Fig. 5C), reduction in the highest branch order ($P < 0.039$; Fig. 5D), reduced number of endings ($P < 0.047$; Fig. 5E) and smaller total surface area ($P < 0.021$; Fig. 5F) of the apical dendrite. For the basal dendrites, we observed the same trends (Fig. 5B–F), but it only reached significance for the total surface area ($P < 0.026$; Fig. 5F). Subsequently, Sholl analysis was performed by placing concentric circles around the cell body and counting the number of intersections (inset Fig. 5H). Apical dendrites of *Ehmt1*$^{+/-}$ neurons had a significantly decreased number of intersections when compared with wild-type neurons (20–360 μm from soma, $F_{1,63} = 5.113$, $P < 0.027$; Fig. 5H). This effect was most apparent at a distance of 60–160 μm from the soma, where the number of intersections, or the number of branches, was the highest ($F_{1,63} = 10.310$, $P < 0.002$; Fig. 5H). For basal dendrites, we observed the same trend,

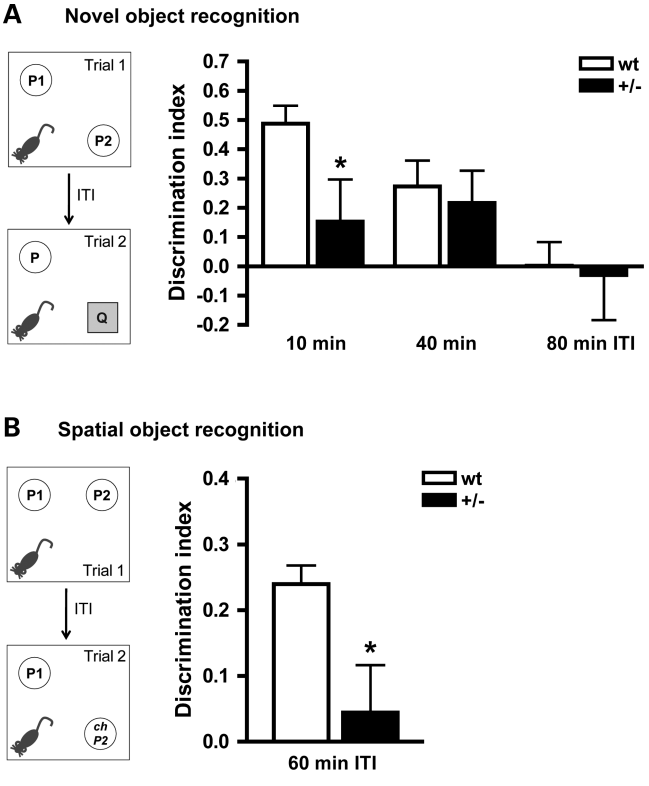

Figure 4. Impaired novel and spatial object recognition memory in *Ehmt1*$^{+/-}$ mice. (**A**) Novel object recognition test. Mice needed to discriminate the new object Q from the familiar object P in trial 2. The discrimination index *d*2 was calculated from the exploration times (s) for objects *P* and *Q* according to the formula: $(Q - P)/(P + Q)$. *Ehmt1*$^{+/-}$ mice ($n = 7$) showed a significantly reduced discrimination index at 10 min ITI when compared with wild-type ($n = 15$). Furthermore, at 80 min ITI both genotypes did not discriminate the new object as indicated by a discrimination index of around 0. (**B**) Spatial object recognition test. Now, mice needed to discriminate the changed location of object P2 (*chP2*) from the non-displaced object P1. The discrimination index *d*2 was calculated from the exploration times (s) for objects P1 and *chP2* according to the formula: $(chP2 - P1)/(P1 + chP2)$. Wild-type mice ($n = 10$) showed clear discrimination between objects P1 and *chP2*, whereas *Ehmt1*$^{+/-}$ mice ($n = 10$) revealed a significantly lower *d*2 value at 60 min ITI. Notably, *Ehmt1*$^{+/-}$ mice did not show any discrimination between P1 and *chP2* as demonstrated by a *d*2 value around 0. $^{*}P < 0.05$, ITI = intertrial interval.

with a significant difference for 60–80 μm ($F_{1,63} = 4.004$, $P < 0.05$; Fig. 5I). Collectively, this indicates that *Ehmt1*$^{+/-}$ neurons show reduced dendritic arborization and complexity, which may have implications for neuronal functioning.

The major sites of excitatory synaptic transmission are the dendritic spines, and morphological alterations of these spines can be associated with altered neuronal functioning. In accordance with this, spine abnormalities are often observed in ID and other brain disorders (55–57). Therefore, the spine density was measured in wild-type and *Ehmt1*$^{+/-}$ CA1 neurons from secondary and tertiary branches of the apical dendrite. Indeed, *Ehmt1*$^{+/-}$ neurons displayed a 15% reduction in the spine density, compared with wild-type ($P < 0.016$; Fig. 5J). In particular, we observed a strong reduction in the stubby and mushroom type spines in *Ehmt1*$^{+/-}$ neurons compared with wild-type ($P < 0.032$, Fig. 5K). These data indicate that next to deficits in learning and memory and diminished dendritic arborization, Ehmt1 haploinsufficiency also clearly reduced dendritic spine density of hippocampal CA1 neurons.

Increased paired-pulse facilitation and reduced number of mEPSCs in *Ehmt1*$^{+/-}$ hippocampal neurons

Because *Ehmt1*$^{+/-}$ mice are impaired in fear extinction learning and both novel and spatial object recognition, and show diminished dendritic branching and spine density, we asked whether this was associated with altered synaptic transmission and its plasticity. Basal synaptic transmission was recorded by stimulation of the Schäffer collaterals and subsequent recording of fEPSPs in the CA1 region using MEA (29). The input–output relationship was comparable between wild-type and *Ehmt1*$^{+/-}$ neurons (Fig. 6A), indicating that there was no significant difference in basal synaptic transmission. Next, we assessed the role of Ehmt1 in LTP, given its importance for learning and memory (58). After LTP induction, we found no differences in both the amplitude and slope of CA1 fEPSPs between the two genotypes (Fig. 6B). Because Ehmt1, through gene regulation, can exert its function both pre- and post-synaptically, we asked whether *Ehmt1*$^{+/-}$ mice displayed any presynaptic phenotype. To this end we studied PPF of post-synaptic responses, a form of short-term plasticity that is inversely related to the presynaptic release probability of neurotransmitters. PPF was assessed by stimulating Schäffer collaterals with an interpulse interval of 50 ms. Facilitation of the fEPSPs was observed in both genotypes; however, we found a significant increase in PPF in *Ehmt1*$^{+/-}$ neurons compared with wild-type, which could be indicative of a reduced presynaptic release probability ($F_{1,53} = 1187$, $P < 0.0011$; Fig. 6C). Lastly, to further assess the effects of Ehmt1 haploinsufficiency on basal synaptic function, we measured mEPSCs of hippocampal CA1 neurons, using whole-cell voltage clamp recordings. The mEPSCs were measured in the presence of tetrodotoxin, picrotoxin and AP-5 in order to specifically measure AMPAR-mediated mEPSCs. Interestingly, we observed a strong decrease in the frequency of mEPSCs in *Ehmt1*$^{+/-}$ neurons ($P < 0.01$), whereas the amplitude was not affected (Fig. 6D). Since the frequency of mEPSCs is associated with presynaptic release probability and/or changes in the amount of synapses, these data corroborate our earlier findings on higher PPF in *Ehmt1*$^{+/-}$ synapses, indicating a potential deficit in presynaptic release probability. In short, we found that *Ehmt1*$^{+/-}$ mice show both morphological and functional abnormalities of CA1 hippocampal neurons that are indicative of both pre- and post-synaptic defects.

DISCUSSION

Here, we report the functional characterization of the *Ehmt1*$^{+/-}$ mice, a construct valid model for Kleefstra syndrome (KS) (59,60). Using behavioural analyses, we observed learning and memory impairments in fear conditioning extinction, novel object recognition and spatial object recognition in the *Ehmt1*$^{+/-}$ mice. Furthermore, we correlated abnormal behaviour to structural and functional

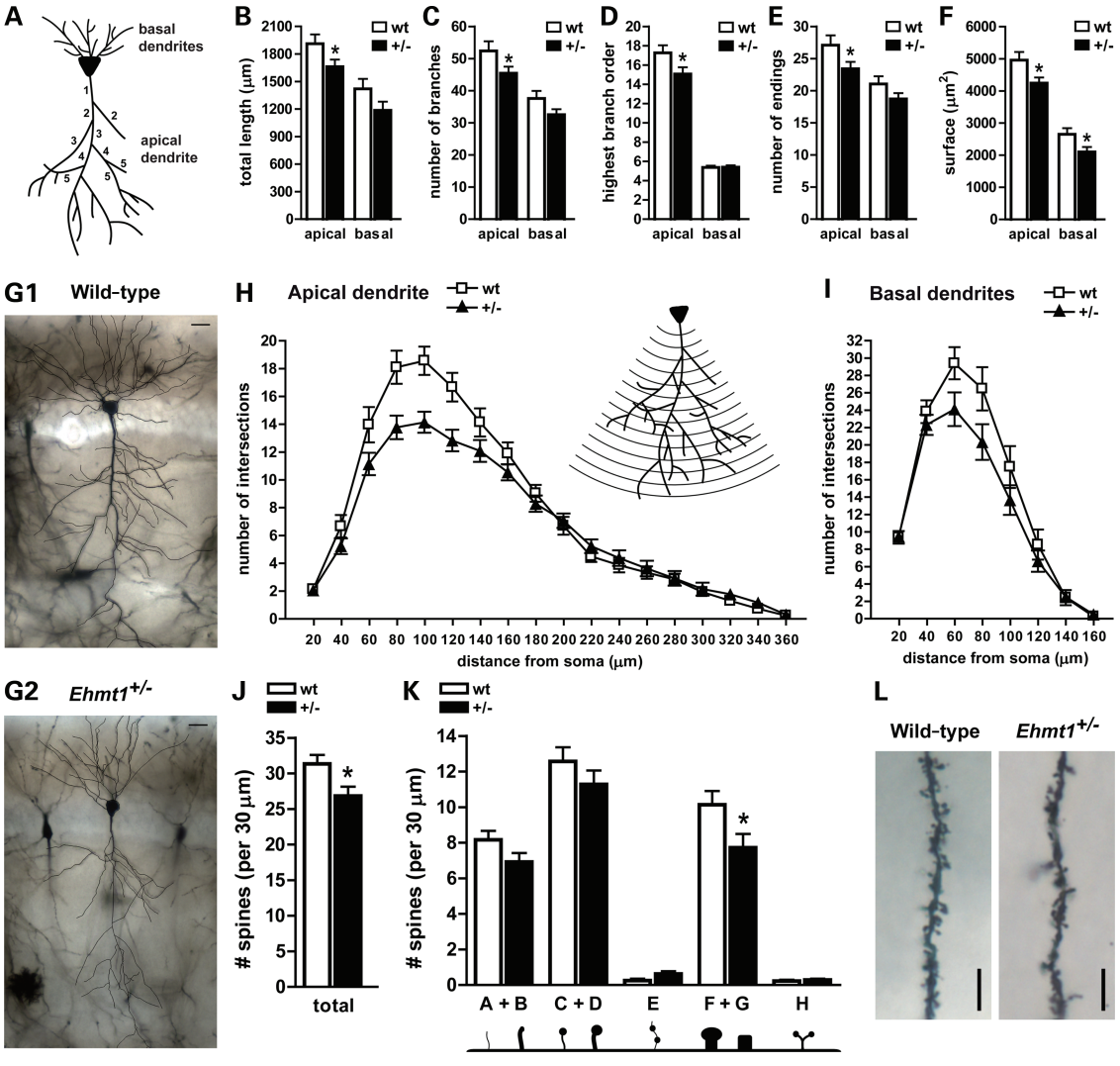

Figure 5. *Ehmt1*$^{+/-}$ neurons show reduced dendritic arborization and reduced spine density. (**A**) Hippocampal CA1 pyramidal neurons were analysed according to centrifugal ordering in panels B–F. Numbers indicate branch order. This branching analysis was performed on wild-type ($n = 30$) and *Ehmt1*$^{+/-}$ ($n = 35$) neurons for apical and basal dendrites separately for the (**B**) total length of all branch parts together, (**C**) number of branch parts, (**D**) highest branch order, (**E**) number of endings, and (**F**) surface area of all branch parts together. (**G1**, **G2**) Representative wild-type and *Ehmt1*$^{+/-}$ neurons, bar = 20 μm. (**H**) For Sholl analysis (inset), concentric circles were placed around the soma and the number of intersections was quantified for wild-type ($n = 30$) and *Ehmt1*$^{+/-}$ ($n = 35$) neurons. *Ehmt1*$^{+/-}$ mice displayed a significantly reduced number of intersections for the apical dendrite. (**I**) The number of intersections following Sholl analysis for the basal dendrites. (**J**) The number of spines was quantified on secondary and tertiary branches of the apical dendrite of CA1 pyramidal neurons, showing a significantly reduced spine density in *Ehmt1*$^{+/-}$ ($n = 33$) compared with wild-type ($n = 30$). (**K**) When spines were quantified according to the morphological category, *Ehmt1*$^{+/-}$ neurons displayed a significantly reduced number of mature, stubby and mushroom, spines. (**L**) Representative images of wild-type and *Ehmt1*$^{+/-}$ branches, bar = 5 μm. $^{*}P < 0.05$.

synaptic deficits. Although the *Ehmt1*$^{+/-}$ mice display no obvious abnormalities in the gross anatomy of the hippocampus, more in-depth analysis of CA1 hippocampal neurons revealed significant reductions in spine density, number of mature spines and dendritic arborization in the *Ehmt1*$^{+/-}$ mice, indicating a post-synaptic deficit. Subsequent functional analysis of CA3-CA1 synapses showed altered short-term plasticity as measured by PPF, and a severely reduced mEPSC frequency, indicating a presynaptic deficit. Taken together, these data show that *Ehmt1* haploinsufficiency in mice leads to learning and memory impairments and functional deficits in hippocampal neurons, providing a possible mechanism for ID in patients with KS.

ID is one of the core features of KS (9), implicating a role for Ehmt1 in cognitive function. Indeed, this study shows that *Ehmt1*$^{+/-}$ mice have impairments in several tests assessing hippocampus-associated cognitive function. First, we noted a deficit in fear extinction learning, which is dependent on the prefrontal cortex, amygdala and hippocampus (41,42). This deficit points at decreased adaptive control over the conditioned fear response (61). The persistently high freezing levels of the *Ehmt1*$^{+/-}$ mice during extinction training suggest reduced cognitive flexibility in these mice. Second, we observed that the *Ehmt1*$^{+/-}$ mice had difficulties discriminating a new object from a familiar one in the novel object recognition test. Third, they were unable to detect the

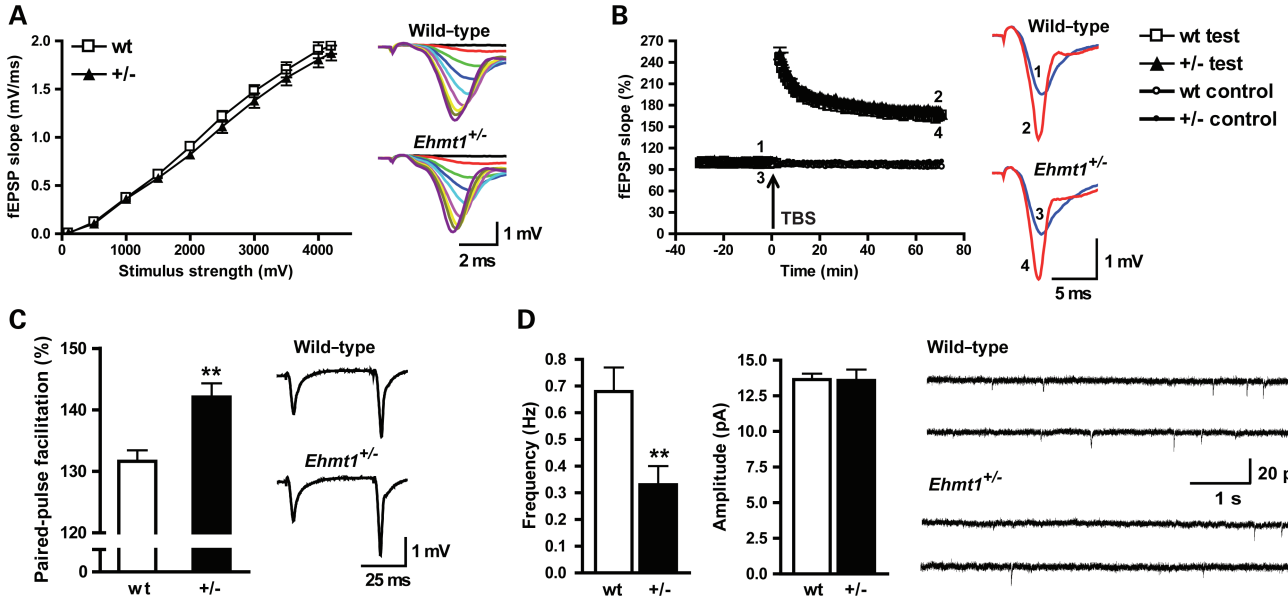

Figure 6. Electrophysiological recordings indicate a presynaptic defect of *Ehmt1*$^{+/-}$ neurons. (**A**) Basal synaptic transmission in wild-type ($n = 32$) and *Ehmt1*$^{+/-}$ ($n = 40$) neurons was recorded by measuring input–output relationships. Schäffer collaterals were stimulated with biphasic voltage pulses of 0.1; 0.5; 1; 1.5; 2; 2.5; 3; 3.5; 4 and 4.2 V, and subsequent recording of fEPSP slopes showed no genotype differences. (**B**) LTP was induced after 30 min of stable baseline fEPSP responses, by a TBS train of 10 bursts given at 5 Hz with four pulses evoked at 100 Hz per burst. Wild-type ($n = 30$) and *Ehmt1*$^{+/-}$ ($n = 40$) neurons showed similar normalized magnitudes of this potentiation. (**C**) PPF was measured by stimulating Schäffer collaterals with a pair of pulses at baseline stimulation strength and an interpulse interval of 50 ms. The % increase in fEPSP slopes was recorded, and this showed a significantly increased facilitation in *Ehmt1*$^{+/-}$ ($n = 40$) neurons compared with wild-type ($n = 32$). (**D**) mEPSCs were recorded in the presence of tetrodotoxin, picrotoxin, and AP-5 from wild-type ($n = 17$) and *Ehmt1*$^{+/-}$ ($n = 14$) neurons, and were significantly reduced in frequency but not in amplitude in the latter. (A)–(D) insets show examples of wild-type and *Ehmt1*$^{+/-}$ traces. $^{**}P < 0.01$, fEPSP = field excitatory post-synaptic potential, mEPSC = miniature excitatory post-synaptic current, LTP = long-term potentiation, TBS = theta-burst stimulation, PPF = paired-pulse facilitation.

displacement of an object in the spatial object recognition test. Both object recognition tests require hippocampus function to a lesser (novel) and a greater (spatial) extent (46–48). On the other hand, the *Ehmt1*$^{+/-}$ mice did not demonstrate learning impairments in the spatial Barnes maze test. The apparent discrepancy of unaffected learning in the Barnes maze is probably explained by its repetitive training protocol. Cognitive impairments were also observed in a *Drosophila* knockout of *EHMT* (23) and in conditional knockout mice, in which *Ehmt1* was homozygously knocked out in postnatal forebrain neurons (22). Taken together, these data indicate an important role for Ehmt1 in cognitive functioning. Two other recent studies specifically investigated the role of the Ehmt1/Ehmt2 complex and the Ehmt1 H3K9 dimethylation mark in fear conditioned learning. Pharmacological inhibition of Ehmt1/Ehmt2 in the entorhinal cortex, but not the hippocampus, enhanced contextual fear conditioning, and induced several other histone methylation and acetylation marks (62). The H3K9 dimethylation mark is triggered in hippocampus during both novel context learning and associative contextual learning of fear (63), which correlates with the reduced exploration in a novel context of the *Ehmt1*$^{+/-}$ mice (18). In addition, histone deacetylase (HDAC) inhibition resulted in significantly decreased H3K9 dimethylation in the hippocampus (63), suggesting a dynamic cross talk between histone methylation and acetylation in the hippocampus. Another recent study found that HDAC1 inhibition in the hippocampus impaired fear extinction (64). Our finding of impaired fear extinction in the *Ehmt1*$^{+/-}$ mice could thus be explained by an altered histone modification equilibrium. The importance of histone modifications in learning and memory function, and the apparently delicate balance, is reflected in a substantial number of genes involved in epigenetic regulation that cause ID when mutated (13,14). Notably, Ehmt2 appears to be part of a repressive complex including HDACs and SMCX/JARID1C together with the neuronal transcriptional repressor REST, underscoring the importance of tightly controlled histone modifications for cognitive functioning (65).

During the fear conditioning test, we noted markedly increased freezing of the *Ehmt1*$^{+/-}$ mice to the footshock during both acquisition and context memory testing. In addition, we found a substantially higher response of the *Ehmt1*$^{+/-}$ mice to an acoustic stimulus. Increased freezing during context memory testing was also observed in the valproic acid rat model for autism (66), and a rat model for post-traumatic stress disorder (PTSD; (67)). In addition, a mouse model for PTSD displayed a significantly increased response to acoustic startle (68), similar to what we observed in the *Ehmt1*$^{+/-}$ mice. The increased anxiety of *Ehmt1*$^{+/-}$ mice (18), which is also a feature of autism (69) and PTSD (DSM-IV criteria), may give us a possible explanation for the increased response to footshock. Indeed, high anxiety mice show an increased acoustic startle response (70,71) and high freezing during contextual fear conditioning (72). In addition, PTSD includes hypervigilance, which is an increased sensitivity to external stimuli, which could cause the increased responsiveness to a loud acoustic stimulus or a painful stimulus like a footshock. Recently it was shown that children with

autism spectrum disorder and ID, and with ID alone that displayed stereotyped behaviour, were significantly more sensitive to sensory information processing (73), which is in line with the observed increased sensitivity reaction of the *Ehmt1*$^{+/-}$ mice. In accordance, fragile X mental retardation protein knockout mice, a model for ID and autism, showed similar sensory hypersensitivity (74). Whereas for KS patients, it is known that they show autistic-like features, but their sensory processing has not yet been investigated (19).

In-depth morphological analysis of *Ehmt1*$^{+/-}$ CA1 hippocampal neurons revealed significantly reduced complexity of dendritic branches. Dendritic abnormalities are observed in most, if not all, ID disorders (51). Usually branches are noted to be shorter or less complex, which is indeed seen in the *Ehmt1*$^{+/-}$ mice. Interestingly, a fly knockout for *EHMT* revealed similarly reduced complexity of sensory neuron branches (23), indicating that this effect of Ehmt1 absence is preserved across species. It is of note that dendritic morphology was reported to be normal in conditional *Ehmt1* knockout mice studied by Schaefer *et al*. (22). This differential dendrite phenotype may reflect an important role of Ehmt1 in embryonic development and in the early postnatal period before ablation of the *Ehmt1* gene in the conditional knockout mice. When focusing on the actual places of synaptic transmission, the dendritic spines, we observed a significantly reduced spine density, and more specifically a reduced number of mature mushroom type spines. Also this reduction in spine density is observed in multiple ID disorders (51,75). The combination of reduced dendritic branching and reduced spine density will probably have large implications for neuronal functioning, as reflected by the learning impairments we observed in the *Ehmt1*$^{+/-}$ mice.

Electrophysiological recordings of the CA3-CA1 Schäffer collaterals showed normal input–output curves in *Ehmt1*$^{+/-}$ neurons, suggesting that there were no drastic effects of Ehmt1 haploinsufficiency on basal synaptic transmission. Furthermore, no changes in LTP were observed in the hippocampus. However, other brain regions like the entorhinal cortex and the amygdala were also involved in the applied learning tests, thus studying LTP in these regions would be very interesting and might reveal altered synaptic transmission there. Interestingly, PPF was significantly enhanced in the hippocampus of *Ehmt1*$^{+/-}$ mice, which is indicative of a reduced presynaptic release probability (76,77). Furthermore, changes in PPF were observed during consecutive extinction sessions of an associative learning task in mice (78), implicating a link between the two. Accordingly, a recent study revealed both increased PPF and impaired fear conditioned extinction learning in mice overexpressing MeCP2 (79), which is similar to our observations in *Ehmt1*$^{+/-}$ mice. To further assess the effects of Ehmt1 haploinsufficiency on basal synaptic function, we measured mEPSCs of CA1 neurons, and demonstrated a significantly reduced frequency of ∼50%, whereas the amplitude was not affected. The reduced presynaptic release probability, as indicated by increased PPF, could attribute to the decreased number of mEPSCs measured in the post-synaptic cell. Thus, the reduced mEPSC frequency corroborates our earlier findings on PPF. Furthermore, the decreased spine density and decreased dendritic arborization might also contribute to the reduced number of mEPSCs. Combined, these data demonstrate that altered Ehmt1 expression significantly affects the synaptic structure and function in the mouse brain. Accordingly, *EHMT1* knockout flies showed a significant loss of H3K9 dimethylation at 5′ and 3′ ends of genes involved in nervous system development, dendrite morphogenesis and signal transduction pathways involved in learning and memory (23).

In summary, *Ehmt1*$^{+/-}$ mice show cognitive impairments that may reflect the ID seen in KS patients, and therefore represent a valuable animal model for further studying this disorder. Morphological and functional analyses of hippocampal synapses revealed both pre- and post-synaptic alterations, indicating an important role for Ehmt1 in neuronal functioning. Our findings provide clues for a mechanism of the cognitive impairments seen in KS. In addition, these results appear to be relevant also for other neurodevelopmental and psychiatric conditions, such as autism spectrum disorder and schizophrenia, for which *de novo EHMT1* mutations were recently identified (15–17).

ANIMALS, MATERIALS AND METHODS

Animals and genotyping

We used *Ehmt1*$^{+/-}$ heterozygous knockout mice (1) and *Ehmt1*$^{+/+}$ wild-type littermates, kept on the C57BL/6J background. The mice were bred, housed and genotyped as described before (18). The novel object recognition test was performed before genotyping, thus the entire litter was tested. At postnatal day (pnd) 28, a small ear perforation was taken for genotyping and identification. All experiments were performed in a blinded fashion.

All procedures involving animals were approved by the Animal Care Committee of the Radboud University Nijmegen Medical Centre, The Netherlands, conforming to the guidelines of the Dutch Council for Animal Care and the European Communities Council Directive of 24 November 1986 (86/609/EEC).

Western blot

Mice of 4, 8, 14 days and 1, 3, 10, 20 months old were sacrificed by cervical dislocation, and either whole brain or cortex and hippocampus were quickly dissected, frozen in liquid nitrogen and stored at −80°C. For 10 mg of tissue, 180 µl of RIPA lysis buffer was added, consisting of 50 mM Tris-HCl pH 8.0, 150 mM NaCl, 0.5% NP40, 0.5% deoxycholate (DOC), 0.1% sodium dodecyl sulphate (SDS), 1 mM phenylmethanesulfonylfluoride and 1× protease inhibitor cocktail (Roche Diagnostics, Mannheim, Germany). The tissue was homogenized, incubated for 20 min on ice and spun down at full speed for 20 min at 4°C. The supernatant was diluted with 2× Laemmli sample buffer and heated at 95°C for 5 min. The samples were subjected to electrophoresis on 8% SDS-polyacrylamide gels and transferred to polyvinylidene difluoride membranes (Immobilon-FL, Millipore). Membranes were blocked for 30 min with 3% bovine serum albumin in tris buffered saline with tween (TBS-T; 10 mM Tris-HCl pH 7.5, 150 mM NaCl, 0.05% Tween-20) and divided into two parts. One part was incubated with a mouse-anti-Ehmt1 antibody

(1:2000, ab41969, Abcam) and the other part with a rabbit-anti-γ-tubulin antibody (1:2000, T5192, Sigma-Aldrich), diluted in blocking buffer, overnight at 4°C. After washes with TBS-T, the membranes were incubated with either a goat-anti-mouse-680 fluorescent secondary antibody (1:20 000; Westburg BV, The Netherlands) or a goat-anti-rabbit-800 antibody (1:20 000; Westburg BV, The Netherlands), diluted in blocking buffer for 1 h at room temperature. After washes with TBS-T, the membranes were scanned with the LI-COR Odyssey Imager (Westburg BV, The Netherlands). Intensities of Ehmt1 protein bands were normalized to the corresponding γ-tubulin intensity.

Barnes maze/12 circular holeboard spatial learning test

Wild-type ($n = 6$ males, $n = 6$ females) and *Ehmt1*$^{+/-}$ mice ($n = 6$ males, $n = 6$ females) of 4 months old were tested on a white circular board (diameter 110 cm), with 12 concentric holes (diameter 4 cm) at a distance of 9 cm from the rim (Barnes maze). For analysis, the board was divided into four quadrants (north west, NW; north east, NE; south east, SE; south west, SW) with three holes each. Four different spatial cues were present at ~30 cm distance from the rim. Mice were placed in the testing room 30 min before testing, and before each mouse the apparatus was thoroughly cleaned with water and dried with a paper towel.

For habituation, 7 days prior to, and during the entire experiment, an s-shaped tube was placed in the home cages of the mice. All mice were handled and habituated to the testing procedure by placing them individually in an open cylinder, positioned around one of the holes, and they had to leave the board via the s-shaped escape tube. The procedure was performed two times per day, for 4 days. The subsequent free exploration trial was performed with all 12 holes closed, and mice were able to explore to board for 2 min. Acquisition consisted of 17 trials which were executed on 9 days (2 trials per day, except for day 9 on which only 1 trial was performed). In these trials, 11 holes were closed and 1 hole (the middle hole of the SE quadrant) was connected to the s-shaped escape tube, at a fixed position with respect to the spatial cues. For 2 min, or until the mouse escaped, the number of errors (incorrect hole visits) and escape latency (time to find the escape hole) were manually scored by an observer. The probe test was performed on the same day as the last learning trial, with all 12 holes closed, for 2 min. An additional long-term probe test was performed 7 days later.

This Barnes maze protocol was repeated with a second group of mice at an older age. Wild-type ($n = 11$) and *Ehmt1*$^{+/-}$ ($n = 11$) female mice (9–11 months old) performed the acquisition phase and probe test, with the long-term probe test after 11 days. During a reversal learning protocol, the mice were subjected to six learning trials, with the escape tube located at the middle hole of the SW quadrant. The last learning trial was followed by a reversal probe trial. The time spent in each of the four quadrants was analysed afterwards from DVD with EthoVision® video tracking software (Noldus Information Technology, The Netherlands).

Fear conditioning test

Wild-type ($n = 13$) and *Ehmt1*$^{+/-}$ ($n = 10$) male mice of 3 months old were tested for contextual and cued fear conditioning. Before testing, the animals were handled for 7 days in order to reduce stress. The mice were housed separately during the experiment. Each mouse was transported to the testing room immediately prior to the start of the trial, and before each mouse the apparatus was thoroughly cleaned with water and dried with a paper towel.

We used the StartFear system (Panlab, S.L.U., Barcelona, Spain) which consisted of a 25 × 25 × 25 cm box with black methacrylate walls, a transparent front door and a grid on the floor, situated on a high-sensitivity weight transducer platform. The setup was placed in a sound-attenuating cubicle. Footshock, background noise, house light and tone were all controlled by Freezing software (v1.3.04 Panlab, S.L.U., Barcelona, Spain). The gain of the weight transducer was set at ×5000, the AC filter at 0.5 Hz and the gain to the computer at ×16. Detection of freezing was done automatically by the software according to the following settings: the activity of the mouse should be at least 1500 ms below a threshold of 5.5 (arbitrary units). Additionally, the investigator kept track of jumping, running and vocalizing responses to the footshock, and amount of faeces and urine. All trials were video recorded.

During all trials, the house light was turned on and the speaker delivered 60 dB white noise. For acquisition, the investigator wore a blue coat and blue gloves and 10% ethanol was applied to the chamber walls. The mouse was allowed to explore the chamber for 2 min. Then, a 85 dB 2800 Hz tone was presented for 30 s that co-terminated with a 1 s 0.5 mA footshock, followed by a 1 min intertrial interval (ITI). This tone–footshock–ITI cycle was repeated three times more. The context test was done 24 h after acquisition in the same black context with 10% ethanol scent. The mice were allowed to explore for 5 min and freezing was automatically detected by the software. Testing for tone association was performed 48 h after acquisition in the same box. However, walls were replaced by white ones and the grid was covered by a white smooth floor, also the transparent front door was made white. The investigator wore a white coat and white gloves and almond scent was applied to the walls. After 2 min free exploration, the 85 dB 2800 Hz tone was presented for 30 s followed by a 1.5 min ITI. This tone–ITI cycle was repeated two times more. Five days after acquisition, we started a tone extinction paradigm, for 6 days, with the white background settings. After 1 min exploration, the 85 dB 2800 Hz tone was presented for 30 s, followed by a 1 min ITI. This tone–ITI cycle was repeated four times more.

Acoustic startle reflex and auditory brainstem response measurements

Male wild-type ($n = 9$) and *Ehmt1*$^{+/-}$ mice ($n = 9$) of 3 months old were tested for their reaction to an acoustic stimulus with a startle response system (SR-LAB, San Diego Instruments, USA). Each mouse was placed in a non-restrictive Plexiglas cylinder (4 cm diameter, 8.5 cm length), resting on a platform that was able to transduce vibrations produced by the whole-body startle response of the mouse. The cylinder

was situated in a sound attenuated chamber containing a speaker that provided the acoustic stimuli and a continuous background noise. The trial started with 5 min habituation to the 70 dB background noise, followed by seven blocks with seven sound levels per block: 70 (no stimulus), 80, 90, 100, 110, 120, 130 dB, presented in a pseudo-random order. The time between two stimuli was 10, 12, 15, 18 or 20 s, also determined pseudo-randomly. Each stimulus was presented for 30 ms and the startle response was measured during a 30 ms period.

A part of these mice ($n = 5$ wild-type and $n = 8$ *Ehmt1*$^{+/-}$ mice) was then tested for their hearing abilities using the ABR measurement as described before (supplemental data of (24)).

Novel object recognition test

Wild-type ($n = 6$ males, $n = 9$ females) and *Ehmt1*$^{+/-}$ mice ($n = 5$ males, $n = 2$ females) of 6 weeks old were tested using the novel object recognition test. We used a square open field (50 × 50 × 40 cm, LxDxH) with white plastic walls. Four different, non-displaceable objects were used. These objects were selected for their equal appeal, based on pilot work with C57BL/6J mice. The objects were available in triplicate to avoid olfactory trails. The open field and objects were cleaned thoroughly with water before each trial. All mice were placed in the test room 30 min before testing. The mice were habituated to the open field 5 min per day, for 2 days.

For training trial 1, the open field contained two identical objects (P1 and P2), placed in two opposite corners 10 cm away from the wall. The mouse was placed in a third corner, and allowed to explore for 5 min. After an ITI of 10, 40 or 80 min, the mouse was placed in the open field again for test trial 2, with two new objects (one similar P and one dissimilar Q). Each mouse performed each ITI with a 48 h interval, and the order of the ITIs was randomized. Also, the location of objects P and Q during trial 2 was determined randomly. For each ITI, the mouse had different objects for P and Q, which could be any of the four available objects. Both trials 1 and 2 (5 min each) were recorded on DVD and object exploration (in seconds) was scored manually by an observer. Exploration was defined as follows: directing the nose to the object at a distance of no more than 2 cm and/or touching the object with the nose. Sitting on the object was not scored as object exploration.

Spatial object recognition test

Wild-type ($n = 5$ males, $n = 5$ females) and *Ehmt1*$^{+/-}$ mice ($n = 4$ males, $n = 6$ females) of 4 months old were tested in the spatial object recognition test, according to (25). The mice were habituated to the open field 5 min per day, for 3 days. For training trial 1, the open field contained two identical objects (P1 and P2) placed in two parallel corners 15 cm away from the wall and each mouse, placed in a third corner, was allowed to explore for 10 min. Trial 2 was performed after an ITI of 60 min, and mice were exploring the open field with object P1 still in the same position and object P2 in a changed location (*chP2*, in the opposite corner of the open field) during 5 min. Spatial cues were the camera on a tripod, black paper covering the window and a green notice board. Both trials 1 (10 min) and 2 (5 min) were recorded on DVD and object exploration (in seconds) was scored manually by two independent observers.

For both novel and spatial object recognition tests, the *d*2 discrimination parameter (26) was calculated. This value represents the discrimination between the new/displaced object and the similar/non-displaced object, including a correction for the total exploration activity of each mouse. This value was calculated by the following formula: (Q-P)/(P+Q) for novel object recognition, or (*chP2*-P1)/(P1+*chP2*) for spatial object recognition with values in time (s).

Golgi staining

Brains of 3 months old male wild-type ($n = 6$) and *Ehmt1*$^{+/-}$ ($n = 7$) mice were quickly removed after decapitation, and placed in Golgi-Cox solution (1.04% potassium dichromate, 1.04% mercury chloride, 0.83% potassium chromate, dissolved in double distilled water) for 3 weeks. The brains were rinsed four times in water for 5 min, and dehydrated in 70% EtOH (O/N), 96% EtOH (O/N), 100% EtOH (8 h) and 1:2 EtOH/ether (O/N). Then, the brains were saturated by consecutive overnight incubations in 3, 6 and 12% celloidin. Celloidin was cleared with chloroform before 200 μm coronal sections were cut. Staining was developed by a 5 min rinse in water, 30 min in 16% ammonia, a 2 min rinse in water, 7 min in 1% sodium thiosulphate and 2 × 5 min rinse in water followed by dehydration for 5 min in 70% EtOH, 5 min in 96% EtOH, 5 min in butanol and 5 min in Histo-clear (Biozym, Landgraaf, The Netherlands). The sections were mounted in Histomount (National Diagnostics, Atlanta, GA, USA) under glass coverslips.

We selected $n = 30$ wild-type and $n = 35$ *Ehmt1*$^{+/-}$ hippocampal CA1 pyramidal neurons (according to (27)). Each neuron was traced with Neurolucida software (version 9, MBF Bioscience, Vermont, USA) with a ×40 objective. The acquired data were analysed with Neurolucida explorer. We performed branching analysis and Sholl analysis, for apical and basal dendrites separately. Branching analysis was done according to centrifugal ordering (see Fig. 5A) to determine the total length of all branch parts together, number of branch parts, the highest branch order, the total number of endings and the total surface area of all branch parts together. For the Sholl analysis, the software placed concentric circles around the cell body spaced 10 μm apart, and the number of intersections was quantified.

Dendritic spine analysis was performed with a ×100 objective on 30 μm long sections of secondary and tertiary branches of the apical dendrite that originated at an 80 μm distance from the soma. Both total number and morphological category (adopted from (28)) were recorded.

Preparation of acute hippocampal slices and organotypic brain slices

Acute hippocampal brain slice preparation was performed as described previously (29). In brief, 7 months old male wild-type ($n = 9$) and *Ehmt1*$^{+/-}$ ($n = 10$) mice were sacrificed by cervical dislocation and the brains were immediately

immersed in ice-cold 'cutting' solution (110 mM sucrose, 60 mM NaCl, 28 mM $NaHCO_3$, 1.25 mM NaH_2PO_4, 3 mM KCl, 7 mM $MgSO_4$, 0.5 mM $CaCl_2$, 5 mM glucose, 0.0015 mM phenol red) gassed with a gas mixture of 95%O_2 and 5%CO_2. Whole brain slices were cut at 350 μm thickness by a Vibroslice MA752 (Campden Instruments, Loughborough, UK) in a way that the blade would cut through hemispheres at an angle of 20–30° to their horizontal planes. 'Cutting' solution in the temperature-controlled Peltier bath was maintained at 0–3°C and constantly saturated with a mixture of 95% O_2 and 5% CO_2. Slices were placed into a well of a slice chamber (Fine Science Tools, Foster City, CA, USA) and kept interfaced between moist air and subfused fresh artificial cerebrospinal fluid (ACSF) that contained 124 mM NaCl, 25 mM $NaHCO_3$, 1 mM NaH_2PO_4, 4.4 mM KCl, 1.2 mM $MgSO_4$, 2 mM $CaCl_2$, 10 mM glucose and 0.0015 mM phenol red. Temperature in the chamber was slowly increased to 30°C for the rest of the incubation time. Slices rested under these conditions for at least 2 to 3 h before experiments commenced.

Organotypic hippocampal slice cultures were prepared from pnd 8 mouse pups (wild-type $n = 3$, *Ehmt1*$^{+/-}$ $n = 3$) as described (30) and used for electrophysiology experiments at 7 to 8 days *in vitro* (DIV).

Experimental settings for electrophysiological measurements

Acute hippocampal slices were used to record field excitatory post-synaptic potentials (fEPSPs), by the MEA60 electrophysiological suite (Multi Channel Systems, Reutlingen, Germany). Eight set-ups consisting of a MEA1060-BC preamplifier and a filter amplifier (gain × 550) were run simultaneously by a data acquisition unit operated by MC_Rack software. Raw electrode data were digitized at 10 kHz and stored on a PC hard disk for subsequent analysis. To record fEPSPs, a hippocampal slice was placed into the well of a 5 × 13 3D multi-electrode array (MEA) biochip (Ayanda Biosystems, Lausanne, Switzerland). The slice was guided to a desired position with a fine paint brush and gently fixed over MEA electrodes by a silver ring with attached nylon mesh lowered vertically by a one-dimensional U-1C micromanipulator (You Ltd, Tokyo, Japan). MEA biochips were fitted into the pre-amplifier case and fresh ACSF was delivered to the MEA well through a temperature-controlled perfusion cannula that warmed perfused media to 32°C. Monopolar stimulation of Schäffer collateral/commissural fibres through array electrodes was performed by a STG4008 stimulus generator (Multi Channel Systems, Reutlingen, Germany). Biphasic (positive/negative, 100 μs/a phase) voltage pulses were used. Amplitude, duration and frequency of stimulation were controlled by MC_Stimulus II software. All long-term potentiation (LTP) experiments were performed using two-pathway stimulation of Schäffer collateral/commissural fibres (31,32). Our previous experiments that utilized MEAs demonstrated that largest LTP was recorded in the proximal part of apical dendrites of CA1 pyramidal neurons (29). We have, therefore, picked a single principal recording electrode in the middle of proximal part of CA1 and assigned two electrodes for stimulation of the control and test pathways on the subicular side and on the CA3 side of SR, respectively. The distance from the recording electrode to the test stimulation electrode was 400–510 μm and to the control stimulation electrode 316–447 μm.

Organotypic hippocampal slice cultures were used to record miniature excitatory post-synaptic currents (mEPSCs) with Multiclamp 700B amplifiers (Axon Instruments). Slices were transferred to the recording chamber which was perfused with ACSF containing 119 mM NaCl, 2.5 mM KCl, 2.5 mM $CaCl_2$, 1 mM $MgCl_2$, 26 mM $NaHCO_3$, 1 mM NaH_2PO_4, 11 mM glucose, 0.1 mM picrotoxin and 4 mM 2-chloroadenosine (pH 7.4), and gassed with 95% O_2 and 5% CO_2. Recordings were made at 30°C. Patch recording pipettes (3–5 mV) were filled with intracellular solution containing 115 mM caesium methanesulfonate, 20 mM CsCl, 10 mM HEPES, 2.5 mM $MgCl_2$, 4 mM Na_2ATP, 0.4 mM Na_3GTP, 10 mM sodium phosphocreatine and 0.6 mM EGTA (pH 7.25). Spontaneous responses were recorded at −60 mV (mEPSC) in ACSF containing 2.5 mM $CaCl_2$ and 1.2 mM $MgCl_2$ at 30°C. mEPSCs were recorded in the presence of 1 mM tetrodotoxin, 0.1 mM picrotoxin and 0.1 mM AP-5.

Electrophysiological data analysis

To evoke orthodromic fEPSPs in the acute slices, stimulation electrodes were activated at a frequency of 0.02 Hz. The 20–80% slope of the negative part of fEPSPs was used as a measure of the synaptic response. Following at least 10–15 min of the equilibration period inside a MEA well, input–output relationships were obtained and baseline stimulation strength was set to evoke a response that corresponded to ∼40% of the maximal attainable fEPSP at the principal recording electrode. Paired-pulse facilitation (PPF) was observed after stimulating Schäffer collateral/commissural fibres with a pair of pulses at baseline stimulation strength and an interpulse interval of 50 ms. The PPF value was calculated as fEPSP2/fEPSP1*100%. Average data from five paired-pulse stimulations were used for each slice. LTP was induced after a 30 min period of stable baseline responses by applying a theta-burst stimulation (TBS) train consisting of 10 bursts given at 5 Hz with four pulses given at 100 Hz per burst. Stimulus strength was not altered during TBS. LTP plots were scaled to the average of the first five baseline points. To account for a possible drift of baseline conditions, the amplitude values in the test pathway were normalized by respective amplitudes in the control pathway prior to statistical comparison. The LTP magnitude was assessed by averaging normalized fEPSPs in the test pathway 60–65 min after TBS episode.

From the organotypic slices, mEPSCs were measured from 5 to 10 min of recordings from each cell. Data were acquired at 10 kHz, filtered at 2 kHz and analysed using the Mini Analysis Program (Synaptosoft).

Statistical analyses

All data are presented as means ± SEM. Unless stated otherwise, the statistical significance of differences between the two groups was assessed using the independent samples

t-test (SPSS 17.0). Barnes maze learning curves, fear conditioning acquisition and extinction data, and Golgi Sholl analysis were tested using a repeated-measures ANOVA (SPSS 17.0). The differences in mEPSCs were assessed by the Mann–Whitney *U* test for unpaired recordings (SPSS 17.0). Input–output relationships were initially compared with mixed model repeated-measures ANOVA and Bonferroni *post-hoc* test implemented in Prism 5 (GraphPad Software, Inc., San Diego, CA, USA) using individual slice data as independent observations. Since several slices were routinely recorded from every mouse, fEPSPmax, PPF and LTP values between wild-type and *Ehmt1*$^{+/-}$ mice were then compared using two-way nested ANOVA design with genotype (group) and mice (sub-group) as fixed effects. Fisher's *F*-statistic was calculated as mean of squares$_{genotype}$/mean of squares$_{residual}$ and the genotype effect was considered significant if the following two conditions were met: (a) the corresponding probability for the group *F*-statistic should be <0.05 and (b) the sub-group effects should be non-significant. For the Barnes maze, novel and spatial object recognition tests, male and female data were analysed separately and, when not significantly different, pooled within a genotype group. For all analyses, the statistical significance was set at $P < 0.05$.

ACKNOWLEDGEMENTS

We would like to thank A. Oudakker (Department of Human Genetics) for genotyping the *Ehmt1*$^{+/-}$ and wild-type mice, J. Dederen (Department of Anatomy) for assistance with the Neurolucida software program, and the employees of the Animal Facilities in Nijmegen and Babraham for their help, advice and animal care.

Conflict of Interest statement. None declared.

FUNDING

This work was supported by the EU FP7 large-scale integrated project GENCODYS (grant 241995) to H.B. and M.K., the MERE-GLU EU FP7 Marie Curie Re-integration Grant (PEOPLE-2010-RG, 277091) to N.N.K., the Dutch brain foundation, KS 2009(1)-122 to T.K. and a grant from the Radboud University Nijmegen Medical Centre (Junioronderzoekerronde 2007) to H.B. and C.E.E.M.V.d.Z.

REFERENCES

1. Tachibana, M., Ueda, J., Fukuda, M., Takeda, N., Ohta, T., Iwanari, H., Sakihama, T., Kodama, T., Hamakubo, T. and Shinkai, Y. (2005) Histone methyltransferases G9a and GLP form heteromeric complexes and are both crucial for methylation of euchromatin at H3-K9. *Genes Dev.*, **19**, 815–826.
2. He, H. and Lehming, N. (2003) Global effects of histone modifications. *Brief. Funct. Genomic Proteomic*, **2**, 234–243.
3. Rice, J.C., Briggs, S.D., Ueberheide, B., Barber, C.M., Shabanowitz, J., Hunt, D.F., Shinkai, Y. and Allis, C.D. (2003) Histone methyltransferases direct different degrees of methylation to define distinct chromatin domains. *Mol. Cell*, **12**, 1591–1598.
4. Ueda, J., Tachibana, M., Ikura, T. and Shinkai, Y. (2006) Zinc finger protein Wiz links G9a/GLP histone methyltransferases to the co-repressor molecule CtBP. *J. Biol. Chem.*, **281**, 20120–20128.
5. Fritsch, L., Robin, P., Mathieu, J.R., Souidi, M., Hinaux, H., Rougeulle, C., Harel-Bellan, A., Ameyar-Zazoua, M. and Ait-Si-Ali, S. (2010) A subset of the histone H3 lysine 9 methyltransferases Suv39h1, G9a, GLP, and SETDB1 participate in a multimeric complex. *Mol. Cell*, **37**, 46–56.
6. Kleefstra, T., Smidt, M., Banning, M.J., Oudakker, A.R., van Esch, H., de Brouwer, A.P., Nillesen, W., Sistermans, E.A., Hamel, B.C., de Bruijn, D. *et al.* (2005) Disruption of the gene euchromatin histone methyl transferase1 (Eu-HMTase1) is associated with the 9q34 subtelomeric deletion syndrome. *J. Med. Genet.*, **42**, 299–306.
7. Kleefstra, T., Brunner, H.G., Amiel, J., Oudakker, A.R., Nillesen, W.M., Magee, A., Genevieve, D., Cormier-Daire, V., van Esch, H., Fryns, J.P. *et al.* (2006) Loss-of-function mutations in euchromatin histone methyl transferase 1 (EHMT1) cause the 9q34 subtelomeric deletion syndrome. *Am. J. Hum. Genet.*, **79**, 370–377.
8. Kleefstra, T., Nillesen, W.M. and Yntema, H.G. (2011) Kleefstra Syndrome. In Pagon, R.A., Bird, T.D., Dolan, C.R. and Stephens, K. (eds), *SourceGeneReviews [Internet]*. Seattle (WA), Seattle: University of Washington.
9. Stewart, D.R. and Kleefstra, T. (2007) The chromosome 9q subtelomere deletion syndrome. *Am. J. Med. Genet. C. Semin. Med. Genet.*, **145C**, 383–392.
10. Willemsen, M.H., Vulto-van Silfhout, A.T., Nillesen, W.M., Wissink-Lindhout, W.M., van, B.H., Philip, N., Berry-Kravis, E.M., Kini, U., van Ravenswaaij-Arts, C.M., Delle, C.B. *et al.* (2012) Update on Kleefstra Syndrome. *Mol. Syndromol.*, **2**, 202–212.
11. Kleefstra, T., Kramer, J.M., Neveling, K., Willemsen, M.H., Koemans, T.S., Vissers, L.E., Wissink-Lindhout, W., Fenckova, M., van den Akker, W.M., Kasri, N.N. *et al.* (2012) Disruption of an EHMT1-associated chromatin-modification module causes intellectual disability. *Am. J. Hum. Genet.*, **91**, 73–82.
12. Kramer, J.M. and van Bokhoven, H. (2009) Genetic and epigenetic defects in mental retardation. *Int. J. Biochem. Cell Biol.*, **41**, 96–107.
13. Nelson, E.D. and Monteggia, L.M. (2011) Epigenetics in the mature mammalian brain: Effects on behavior and synaptic transmission. *Neurobiol. Learn. Mem.*, **96**, 53–60.
14. van Bokhoven, H. and Kramer, J.M. (2010) Disruption of the epigenetic code: an emerging mechanism in mental retardation. *Neurobiol. Dis.*, **39**, 3–12.
15. Kirov, G., Pocklington, A.J., Holmans, P., Ivanov, D., Ikeda, M., Ruderfer, D., Moran, J., Chambert, K., Toncheva, D., Georgieva, L. *et al.* (2012) De novo CNV analysis implicates specific abnormalities of postsynaptic signalling complexes in the pathogenesis of schizophrenia. *Mol. Psychiatry*, **17**, 142–153.
16. Talkowski, M.E., Rosenfeld, J.A., Blumenthal, I., Pillalamarri, V., Chiang, C., Heilbut, A., Ernst, C., Hanscom, C., Rossin, E., Lindgren, A.M. *et al.* (2012) Sequencing chromosomal abnormalities reveals neurodevelopmental loci that confer risk across diagnostic boundaries. *Cell*, **149**, 525–537.
17. O'Roak, B.J., Vives, L., Girirajan, S., Karakoc, E., Krumm, N., Coe, B.P., Levy, R., Ko, A., Lee, C., Smith, J.D. *et al.* (2012) Sporadic autism exomes reveal a highly interconnected protein network of de novo mutations. *Nature*, **485**, 246–250.
18. Balemans, M.C., Huibers, M.M., Eikelenboom, N.W., Kuipers, A.J., van Summeren, R.C., Pijpers, M.M., Tachibana, M., Shinkai, Y., van Bokhoven, H. and Van der Zee, C.E. (2010) Reduced exploration, increased anxiety, and altered social behavior: autistic-like features of euchromatin histone methyltransferase 1 heterozygous knockout mice. *Behav. Brain Res.*, **208**, 47–55.
19. Kleefstra, T., van Zelst-Stams, W.A., Nillesen, W.M., Cormier-Daire, V., Houge, G., Foulds, N., van Dooren, M., Willemsen, M.H., Pfundt, R., Turner, A. *et al.* (2009) Further clinical and molecular delineation of the 9q subtelomeric deletion syndrome supports a major contribution of EHMT1 haploinsufficiency to the core phenotype. *J. Med. Genet.*, **46**, 598–606.
20. Unique Kleefstra syndrome leaflet (2009) www.rarechromo.org/forum/DisordersLeaflets.asp.
21. Verhoeven, W.M., Kleefstra, T. and Egger, J.I. (2010) Behavioral phenotype in the 9q subtelomeric deletion syndrome: a report about two adult patients. *Am. J. Med. Genet. B: Neuropsychiatry Genet.*, **153B**, 536–541.
22. Schaefer, A., Sampath, S.C., Intrator, A., Min, A., Gertler, T.S., Surmeier, D.J., Tarakhovsky, A. and Greengard, P. (2009) Control of cognition and

adaptive behavior by the GLP/G9a epigenetic suppressor complex. *Neuron*, **64**, 678–691.
23. Kramer, J.M., Kochinke, K., Oortveld, M.A., Marks, H., Kramer, D., de Jong, E.K., Asztalos, Z., Westwood, J.T., Stunnenberg, H.G., Sokolowski, M.B. *et al.* (2011) Epigenetic regulation of learning and memory by Drosophila EHMT/G9a. *PLoS. Biol.*, **9**, e1000569.
24. Shin, J.B., Streijger, F., Beynon, A., Peters, T., Gadzala, L., McMillen, D., Bystrom, C., Van der Zee, C.E., Wallimann, T. and Gillespie, P.G. (2007) Hair bundles are specialized for ATP delivery via creatine kinase. *Neuron*, **53**, 371–386.
25. Roozendaal, B., Hernandez, A., Cabrera, S.M., Hagewoud, R., Malvaez, M., Stefanko, D.P., Haettig, J. and Wood, M.A. (2010) Membrane-associated glucocorticoid activity is necessary for modulation of long-term memory via chromatin modification. *J. Neurosci.*, **30**, 5037–5046.
26. Prickaerts, J., van Staveren, W.C., Sik, A., Markerink-van, I.M., Niewohner, U., van der Staay, F.J., Blokland, A. and de, V.J. (2002) Effects of two selective phosphodiesterase type 5 inhibitors, sildenafil and vardenafil, on object recognition memory and hippocampal cyclic GMP levels in the rat. *Neuroscience*, **113**, 351–361.
27. Ramakers, G.J., Wolfer, D., Rosenberger, G., Kuchenbecker, K., Kreienkamp, H.J., Prange-Kiel, J., Rune, G., Richter, K., Langnaese, K., Masneuf, S. *et al.* (2012) Dysregulation of Rho GTPases in the alphaPix/Arhgef6 mouse model of X-linked intellectual disability is paralleled by impaired structural and synaptic plasticity and cognitive deficits. *Hum. Mol. Genet.*, **21**, 268–286.
28. Irwin, S.A., Patel, B., Idupulapati, M., Harris, J.B., Crisostomo, R.A., Larsen, B.P., Kooy, F., Willems, P.J., Cras, P., Kozlowski, P.B. *et al.* (2001) Abnormal dendritic spine characteristics in the temporal and visual cortices of patients with fragile-X syndrome: a quantitative examination. *Am. J. Med. Genet.*, **98**, 161–167.
29. Kopanitsa, M.V., Afinowi, N.O. and Grant, S.G. (2006) Recording long-term potentiation of synaptic transmission by three-dimensional multi-electrode arrays. *BMC. Neurosci.*, **7**, 61.
30. Nadif Kasri, N., Nakano-Kobayashi, A. and Van Aelst, L. (2011) Rapid synthesis of the X-linked mental retardation protein OPHN1 mediates mGluR-dependent LTD through interaction with the endocytic machinery. *Neuron*, **72**, 300–315.
31. Andersen, P., Sundberg, S.H., Sveen, O. and Wigstrom, H. (1977) Specific long-lasting potentiation of synaptic transmission in hippocampal slices. *Nature*, **266**, 736–737.
32. Schwartzkroin, P.A. and Wester, K. (1975) Long-lasting facilitation of a synaptic potential following tetanization in the in vitro hippocampal slice. *Brain Res.*, **89**, 107–119.
33. Barnes, C.A. (1979) Memory deficits associated with senescence: a neurophysiological and behavioral study in the rat. *J. Comp. Physiol. Psychol.*, **93**, 74–104.
34. Streijger, F., Oerlemans, F., Ellenbroek, B.A., Jost, C.R., Wieringa, B. and Van der Zee, C.E. (2005) Structural and behavioural consequences of double deficiency for creatine kinases BCK and UbCKmit. *Behav. Brain Res.*, **157**, 219–234.
35. Lang, S., Kroll, A., Lipinski, S.J., Wessa, M., Ridder, S., Christmann, C., Schad, L.R. and Flor, H. (2009) Context conditioning and extinction in humans: differential contribution of the hippocampus, amygdala and prefrontal cortex. *Eur. J. Neurosci.*, **29**, 823–832.
36. Maren, S. (2008) Pavlovian fear conditioning as a behavioral assay for hippocampus and amygdala function: cautions and caveats. *Eur. J. Neurosci.*, **28**, 1661–1666.
37. Phillips, R.G. and LeDoux, J.E. (1992) Differential contribution of amygdala and hippocampus to cued and contextual fear conditioning. *Behav. Neurosci.*, **106**, 274–285.
38. Abumaria, N., Yin, B., Zhang, L., Li, X.Y., Chen, T., Descalzi, G., Zhao, L., Ahn, M., Luo, L., Ran, C. *et al.* (2011) Effects of elevation of brain magnesium on fear conditioning, fear extinction, and synaptic plasticity in the infralimbic prefrontal cortex and lateral amygdala. *J. Neurosci.*, **31**, 14871–14881.
39. Morgan, M.A. and LeDoux, J.E. (1995) Differential contribution of dorsal and ventral medial prefrontal cortex to the acquisition and extinction of conditioned fear in rats. *Behav. Neurosci.*, **109**, 681–688.
40. Robleto, K., Poulos, A.M. and Thompson, R.F. (2004) Brain mechanisms of extinction of the classically conditioned eyeblink response. *Learn. Mem.*, **11**, 517–524.
41. Sotres-Bayon, F., Bush, D.E. and LeDoux, J.E. (2004) Emotional perseveration: an update on prefrontal-amygdala interactions in fear extinction. *Learn. Mem.*, **11**, 525–535.
42. Bouton, M.E., Westbrook, R.F., Corcoran, K.A. and Maren, S. (2006) Contextual and temporal modulation of extinction: behavioral and biological mechanisms. *Biol. Psychiatry*, **60**, 352–360.
43. Ennaceur, A. and Delacour, J. (1988) A new one-trial test for neurobiological studies of memory in rats. 1: Behavioral data. *Behav. Brain Res.*, **31**, 47–59.
44. Sik, A., van Nieuwehuyzen, P., Prickaerts, J. and Blokland, A. (2003) Performance of different mouse strains in an object recognition task. *Behav. Brain Res.*, **147**, 49–54.
45. Kolkman, M.J., Streijger, F., Linkels, M., Bloemen, M., Heeren, D.J., Hendriks, W.J. and Van der Zee, C.E. (2004) Mice lacking leukocyte common antigen-related (LAR) protein tyrosine phosphatase domains demonstrate spatial learning impairment in the two-trial water maze and hyperactivity in multiple behavioural tests. *Behav. Brain Res.*, **154**, 171–182.
46. Albasser, M.M., Poirier, G.L. and Aggleton, J.P. (2010) Qualitatively different modes of perirhinal-hippocampal engagement when rats explore novel vs. familiar objects as revealed by c-Fos imaging. *Eur. J. Neurosci.*, **31**, 134–147.
47. Broadbent, N.J., Squire, L.R. and Clark, R.E. (2004) Spatial memory, recognition memory, and the hippocampus. *Proc. Natl Acad. Sci. USA*, **101**, 14515–14520.
48. Barker, G.R. and Warburton, E.C. (2011) When is the hippocampus involved in recognition memory? *J. Neurosci.*, **31**, 10721–10731.
49. Bertaina-Anglade, V., Enjuanes, E., Morillon, D. and Drieu la, R.C. (2006) The object recognition task in rats and mice: a simple and rapid model in safety pharmacology to detect amnesic properties of a new chemical entity. *J. Pharmacol. Toxicol. Methods*, **54**, 99–105.
50. Auerbach, B.D., Osterweil, E.K. and Bear, M.F. (2011) Mutations causing syndromic autism define an axis of synaptic pathophysiology. *Nature*, **480**, 63–68.
51. Kaufmann, W.E. and Moser, H.W. (2000) Dendritic anomalies in disorders associated with mental retardation. *Cereb. Cortex*, **10**, 981–991.
52. Mercaldo, V., Descalzi, G. and Zhuo, M. (2009) Fragile X mental retardation protein in learning-related synaptic plasticity. *Mol. Cells*, **28**, 501–507.
53. van Bokhoven, H. (2011) Genetic and epigenetic networks in intellectual disabilities. *Annu. Rev. Genet.*, **45**, 81–104.
54. Pavlowsky, A., Chelly, J. and Billuart, P. (2012) Emerging major synaptic signaling pathways involved in intellectual disability. *Mol. Psychiatry.*, **17**, 682–693.
55. Chapleau, C.A., Calfa, G.D., Lane, M.C., Albertson, A.J., Larimore, J.L., Kudo, S., Armstrong, D.L., Percy, A.K. and Pozzo-Miller, L. (2009) Dendritic spine pathologies in hippocampal pyramidal neurons from Rett syndrome brain and after expression of Rett-associated MECP2 mutations. *Neurobiol. Dis.*, **35**, 219–233.
56. Nadif Kasri, N., Nakano-Kobayashi, A., Malinow, R., Li, B. and Van, A.L. (2009) The Rho-linked mental retardation protein oligophrenin-1 controls synapse maturation and plasticity by stabilizing AMPA receptors. *Genes Dev.*, **23**, 1289–1302.
57. He, C.X. and Portera-Cailliau, C. (2012) The trouble with spines in fragile X syndrome: density, maturity and plasticity. *Neuroscience* http://dx.doi.org/10.1016/j.neuroscience.2012.03.049.
58. Martin, S.J. and Morris, R.G. (2002) New life in an old idea: the synaptic plasticity and memory hypothesis revisited. *Hippocampus*, **12**, 609–636.
59. Nestler, E.J. and Hyman, S.E. (2010) Animal models of neuropsychiatric disorders. *Nat. Neurosci.*, **13**, 1161–1169.
60. Chadman, K.K., Yang, M. and Crawley, J.N. (2009) Criteria for validating mouse models of psychiatric diseases. *Am. J. Med. Genet. B. Neuropsychiatry Genet.*, **150B**, 1–11.
61. Herry, C., Ferraguti, F., Singewald, N., Letzkus, J.J., Ehrlich, I. and Luthi, A. (2010) Neuronal circuits of fear extinction. *Eur. J. Neurosci.*, **31**, 599–612.
62. Gupta-Agarwal, S., Franklin, A.V., Deramus, T., Wheelock, M., Davis, R.L., McMahon, L.L. and Lubin, F.D. (2012) G9a/GLP histone lysine dimethyltransferase complex activity in the Hippocampus and the Entorhinal cortex is required for gene activation and silencing during memory consolidation. *J. Neurosci.*, **32**, 5440–5453.

63. Gupta, S., Kim, S.Y., Artis, S., Molfese, D.L., Schumacher, A., Sweatt, J.D., Paylor, R.E. and Lubin, F.D. (2010) Histone methylation regulates memory formation. *J. Neurosci.*, **30**, 3589–3599.
64. Bahari-Javan, S., Maddalena, A., Kerimoglu, C., Wittnam, J., Held, T., Bahr, M., Burkhardt, S., Delalle, I., Kugler, S., Fischer, A. and Sananbenesi, F. (2012) HDAC1 regulates fear extinction in mice. *J. Neurosci.*, **32**, 5062–5073.
65. Tahiliani, M., Mei, P., Fang, R., Leonor, T., Rutenberg, M., Shimizu, F., Li, J., Rao, A. and Shi, Y. (2007) The histone H3K4 demethylase SMCX links REST target genes to X-linked mental retardation. *Nature*, **447**, 601–605.
66. Markram, K., Rinaldi, T., La, M.D., Sandi, C. and Markram, H. (2008) Abnormal fear conditioning and amygdala processing in an animal model of autism. *Neuropsychopharmacology*, **33**, 901–912.
67. Imanaka, A., Morinobu, S., Toki, S. and Yamawaki, S. (2006) Importance of early environment in the development of post-traumatic stress disorder-like behaviors. *Behav. Brain Res.*, **173**, 129–137.
68. Pynoos, R.S., Ritzmann, R.F., Steinberg, A.M., Goenjian, A. and Prisecaru, I. (1996) A behavioral animal model of posttraumatic stress disorder featuring repeated exposure to situational reminders. *Biol. Psychiatry*, **39**, 129–134.
69. White, S.W., Oswald, D., Ollendick, T. and Scahill, L. (2009) Anxiety in children and adolescents with autism spectrum disorders. *Clin. Psychol. Rev.*, **29**, 216–229.
70. Plappert, C.F. and Pilz, P.K. (2002) Difference in anxiety and sensitization of the acoustic startle response between the two inbred mouse strains BALB/cAN and DBA/2N. *Genes Brain Behav.*, **1**, 178–186.
71. Roy, V., Merali, Z., Poulter, M.O. and Anisman, H. (2007) Anxiety responses, plasma corticosterone and central monoamine variations elicited by stressors in reactive and nonreactive mice and their reciprocal F1 hybrids. *Behav. Brain Res.*, **185**, 49–58.
72. Ponder, C.A., Kliethermes, C.L., Drew, M.R., Muller, J., Das, K., Risbrough, V.B., Crabbe, J.C., Gilliam, T.C. and Palmer, A.A. (2007) Selection for contextual fear conditioning affects anxiety-like behaviors and gene expression. *Genes Brain Behav.*, **6**, 736–749.
73. Joosten, A.V. and Bundy, A.C. (2010) Sensory processing and stereotypical and repetitive behaviour in children with autism and intellectual disability. *Aust. Occup. Ther. J.*, **57**, 366–372.
74. Chen, L. and Toth, M. (2001) Fragile X mice develop sensory hyperreactivity to auditory stimuli. *Neuroscience*, **103**, 1043–1050.
75. Fiala, J.C., Spacek, J. and Harris, K.M. (2002) Dendritic spine pathology: cause or consequence of neurological disorders? *Brain Res. Brain Res. Rev.*, **39**, 29–54.
76. Ramirez, D.M. and Kavalali, E.T. (2011) Differential regulation of spontaneous and evoked neurotransmitter release at central synapses. *Curr. Opin. Neurobiol.*, **21**, 275–282.
77. Zucker, R.S. and Regehr, W.G. (2002) Short-term synaptic plasticity. *Annu. Rev. Physiol.*, **64**, 355–405.
78. Madronal, N., Gruart, A. and Delgado-Garcia, J.M. (2009) Differing presynaptic contributions to LTP and associative learning in behaving mice. *Front Behav. Neurosci.*, **3**, 7.
79. Na, E.S., Nelson, E.D., Adachi, M., Autry, A.E., Mahgoub, M.A., Kavalali, E.T. and Monteggia, L.M. (2012) A mouse model for MeCP2 duplication syndrome: MeCP2 overexpression impairs learning and memory and synaptic transmission. *J. Neurosci.*, **32**, 3109–3117.